Monte Carlo phase diagram for diblock copolymer melts

M. W. Matsen[a] and G. H. Griffiths
Department of Physics, University of Reading, Whiteknights, Reading RG6 6AF, United Kingdom

R. A. Wickham and O. N. Vassiliev[b]
Department of Physics, St. Francis Xavier University, Antigonish, Nova Scotia B2G 2W5, Canada

(Received 14 September 2005; accepted 27 October 2005; published online 10 January 2006)

A partial phase diagram is constructed for diblock copolymer melts using lattice-based Monte Carlo simulations. This is done by locating the order-disorder transition (ODT) with the aid of a recently proposed order parameter and identifying the ordered phase over a wide range of copolymer compositions ($0.2 \leqslant f \leqslant 0.8$). Consistent with experiments, the disordered phase is found to exhibit direct first-order transitions to each of the ordered morphologies. This includes the spontaneous formation of a perforated-lamellar phase, which presumably forms in place of the gyroid morphology due to finite-size and/or nonequilibrium effects. Also included in our study is a detailed examination of disordered cylinder-forming ($f=0.3$) diblock copolymers, revealing a substantial degree of pretransitional chain stretching and short-range order that set in well before the ODT, as observed previously in analogous studies on lamellar-forming ($f=0.5$) molecules. © *2006 American Institute of Physics*. [DOI: 10.1063/1.2140286]

I. INTRODUCTION

Block copolymer research has progressed enormously over the last decade to the point where there is impressive agreement between experiment and theory.[1] Although the agreement extends to a wide spectrum of architectures, the simple *AB* diblock copolymer provides the model system against which this progress is generally measured. Early experimental phase diagrams,[2] such as the one in Fig. 1(a), display five ordered morphologies: the three classical lamellar (L), cylindrical (C), and spherical (S) phases and the two complex gyroid (G) and perforated-lamellar (PL) phases. This is in reasonable agreement with the predicted diagram in Fig. 1(b) calculated by self-consistent-field theory (SCFT),[3] apart from the absence of the PL phase. However, this discrepancy has now been resolved by careful experiments,[4] demonstrating that PL is just a metastable state that eventually converts to the *G* morphology.

Despite the agreement with respect to the selection of phases and the sequence in which they occur, there remain some significant differences between the experimental and theoretical phase diagrams in Fig. 1. First, there is an asymmetry in the experimental diagram about the $f=0.5$ plane usually attributed to conformational asymmetry between the *A* and *B* segments, but this can be easily accounted for by the theory.[5] The remaining differences are largely attributed to fluctuation effects that are ignored by SCFT. It is understood that so-called Brazovskii fluctuations[6] disrupt the weakly segregated morphologies near the mean-field critical point, causing them to be consumed by the disordered phase. This pushes up the order-disorder transition (ODT), creating direct transitions with each of the ordered phases, as observed by experiments. Similarly, the long-range periodic order of the close-packed spherical (S_{cp}) phase, predicted by SCFT, is also disrupted by thermal fluctuations, transforming it into part of the disordered region.[7]

Much of our understanding of fluctuation effects stems from a seminal paper by Fredrickson and Helfand,[8] where they incorporated Brazovskii fluctuations using a Landau-Ginzburg free-energy functional for weakly segregated melts.[9] However, this functional was obtained by mean-field theory, and so the treatment is not necessarily reliable. Indeed, it does not capture the significant degree of pretransitional chain stretching observed in experiments[10] and Monte Carlo simulations.[11] Another concern is a recent demonstration that the approach produces sensible results only because of a mathematical approximation to the free-energy functional.[12] Fortunately, more rigorous field-theoretic simulations are now being developed, but these have so far been restricted to two dimensions.[13] It will be necessary to extend them to three dimensions, as it is well understood that fluctuation effects are, in general, highly sensitive to the dimensionality of the system. For the time being, the feasibility of large-scale three-dimensional simulations is generally achieved by constraining polymer configurations to an artificial lattice.[11,14–21] While these lattice-based approaches have been proven to be very efficient, a definitive detection of the ODT has been problematic.[11,14–18] However, this difficulty has now been overcome with the recent introduction of a new order parameter.[19]

Here we extend the lattice-based Monte Carlo work in Ref. 19, which carefully examined fluctuation effects in disordered melts of diblock copolymer with the symmetric composition $f=0.5$. The present study begins with an analogous series of simulations for asymmetric molecules with $f=0.3$. This is then followed by simulations over a wide

[a]Author to whom correspondence should be addressed. Electronic mail: m.w.matsen@reading.ac.uk
[b]Present address: Department of Radiation Physics, University of Texas, Houston, Texas 77030.

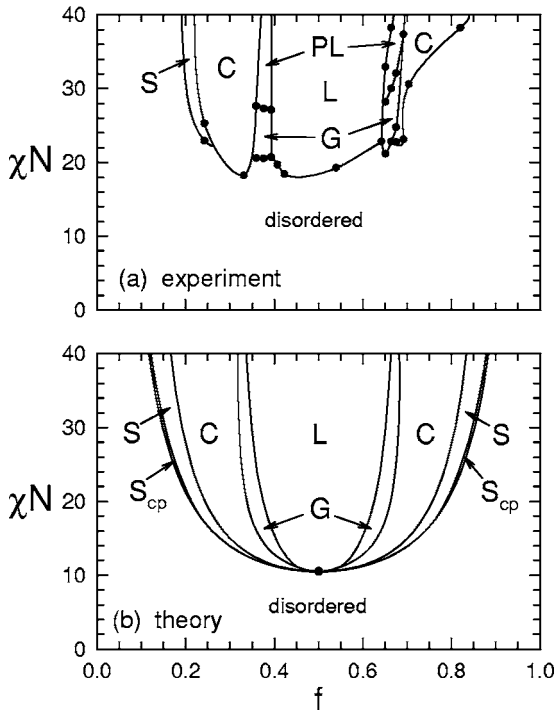

FIG. 1. (a) Experimental (Ref. 2) and (b) theoretical (Ref. 3) phase diagrams measured using polystyrene-polyisoprene diblock copolymers and calculated using SCFT. In (a), the solid dots denote the experimental data points, while the curves serve only as a guide to the eye. In (b), the solid dot marks the mean-field critical point where the L, C, and S regions all merge.

range of compositions ($0.2 \leqslant f \leqslant 0.8$), from which we accurately locate the ODT and identify the geometries of the ordered phases. The results are summarized in the form of a phase diagram for convenient comparison with those in Fig. 1.

II. MONTE CARLO ALGORITHM

A detailed description of the Monte Carlo algorithm used to generate our simulations is provided in Ref. 19. Here we present a summary of its main features, sufficient to interpret our results. In short, the algorithm uses an fcc lattice containing n identical AB diblock copolymer molecules, each formed from N_A A-type monomers joined to N_B B-type monomers. The face-centered-cubic lattice is obtained by taking an $L\times L\times L$ grid with lattice constant d and deleting every second site so that each of the remaining $V\equiv L^3/2$ sites has $z=12$ nearest neighbors separated by a distance of $b=\sqrt{2}d$. The polymer chains are placed on the lattice, assuming periodic boundary conditions with no more than one monomer per site and with each pair of bonded monomers occupying nearest-neighbor sites. To allow room for the polymers to move, the lattice is only partially filled to a copolymer occupancy of $\phi_c \equiv nN/V \approx 0.8$, where $N\equiv N_A+N_B$. The only molecular interactions are between neighboring A and B monomers, where the interaction strength is ϵ_{AB} from which we define a dimensionless Flory-Huggins parameter

$$\chi \equiv \frac{z\epsilon_{AB}}{k_B T}. \tag{1}$$

Although analogous to the χ parameter defined for the continuum Gaussian chain model[22] used by SCFT in Fig. 1(b), this definition is specific to lattice models.

For a given L, N_A, and N_B, our standard simulation begins with a cooling run starting in the disordered phase at $\chi=0$ and stepping up in small increments, $\Delta\chi$, until the system has formed a well-ordered morphology. This is then followed by a heating run back into the disordered state. After each increment in χ, the system is equilibrated with typically 4×10^4 Monte Carlo steps (MCS) per monomer. Each MCS attempts to change the configuration of the system by altering one or two of the copolymers according to the standard Metropolis acceptance criterion.[23] Four types of move are permitted: the slithering snake, chain reversal, crankshaft, and block exchange. After the relaxation period, we generally perform a further 4×10^4 MCS per monomer from which we evaluate various thermodynamic averages by sampling one configuration every 20 MCS per monomer.

The simplest quantity we evaluate is the internal energy $U=\epsilon_{AB}\langle n_{AB}\rangle$, where n_{AB} is the total number of A/B contacts and the angle brackets denote Monte Carlo averages. The heat capacity is also easily calculated using $C_V=(\epsilon_{AB}^2\langle n_{AB}^2\rangle - U^2)/k_B T^2$. A series of structural quantities are evaluated to monitor distortions in the average polymer configuration. These include the radius of gyration of the entire molecule R_g, the radii of gyration of its individual blocks $R_{g,A}$ and $R_{g,B}$, and the average separation between the centers of mass of the A and B blocks R_{AB}. To quantify the domain structure of the melt, we evaluate the correlation function

$$G_{ij} = \langle \sigma_i \sigma_j \rangle - \langle \sigma_i \rangle^2, \tag{2}$$

where $\sigma_i=1$, 0, or -1 if the ith lattice site is occupied by an A monomer, a vacancy, or a B monomer, respectively. From the correlation function, we obtain the structure function

$$S(\mathbf{q}) = \frac{1}{V}\sum_{ij} G_{ij} \exp[i\mathbf{q}\cdot(\mathbf{r}_i - \mathbf{r}_j)], \tag{3}$$

which corresponds to the pattern observed in small-angle scattering experiments.

As mentioned in the Introduction, past studies have struggled to locate the ODT despite the fact that the transition must be first order. All the usual thermodynamic quantities should exhibit discontinuities at the ODT, but they are evidently so small as to be obscured by the statistical noise. Hence, we are in need of an alternative *order parameter* with a more pronounced sensitivity to the ODT. We are not concerned whether or not it has a simple physical interpretation, but it should ideally be zero (or at least very small) in the disordered phase and large in the ordered phase. Reference 19 recently demonstrated that

$$\psi = \frac{1}{V^2}\sum_{i\neq j} G_{ij}^2 \tag{4}$$

serves this requirement for symmetric diblock copolymer melts. Here, we will find that ψ also continues to function as

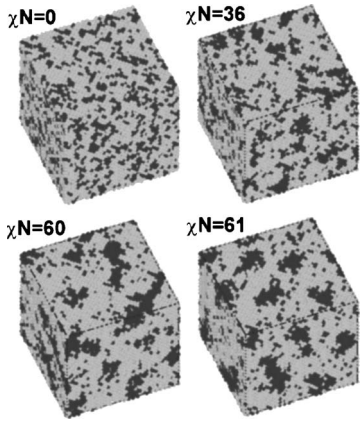

FIG. 2. Configurations taken at $\chi N=0$, 36, 60 (disordered), and 61 (cylindrical) from a Monte Carlo heating run involving diblocks of $N=30$ monomers and composition of $f=0.3$ on a lattice of size $L=50$. The A and B monomers are denoted by dark and light spheres, respectively, while the vacancies have been omitted.

an effective order parameter for asymmetric molecules. It works because the double summation is proportional to V in the disordered state on account of the short-range correlation length, whereas the sum becomes proportional to V^2 when the system develops a long-range order. (Note that G_{ij} is squared simply to avoid the partial cancellation that occurs in the sum due to the oscillating sign it exhibits for periodically ordered morphologies.) Thus for large system sizes, ψ approaches zero in the disordered state, but remains finite for the ordered phases. Unlike order parameters that are based on the composition profile, this ψ also has the convenient property that it is completely unaffected by a simple spatial translation of the morphology.

III. RESULTS FOR $f=0.3$ DIBLOCK COPOLYMERS

Here we perform a detailed examination of cylinder-forming diblocks of composition $f \equiv N_A/N=0.3$, analogous to the previous one for the symmetric case of $f=0.5$.[19] The study is done over a range of molecular weights, $N=20$, 30, and 40, each examined with four different system sizes L in order to assess finite-size effects. The aim is to detect the effect of molecular weight on the position of the ODT and to examine departures from mean-field theory. We specifically test the mean-field assumption of random mixing in the homogeneous disordered phase, which implies that the internal energy U remains constant, the polymer chains conform to random-walk statistics, and the structure function $S(q)$ exhibits a peak at constant wave number q^*.

A. Order parameter

To illustrate the difficulty in locating the ODT, Fig. 2 shows four configurations taken during a heating run performed on asymmetric diblocks of $f=0.3$. Although it is virtually impossible to detect from this diagram, the system switches from an ordered cylinder (C) morphology to the disordered state as χN is stepped from 61 to 60. This slight variation in χN produces virtually no change in the degree of segregation or the characteristic domain size, but it nevertheless produces a dramatic change in the domain geometry.

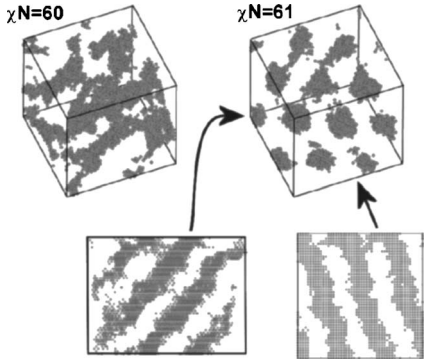

FIG. 3. The $\chi N=60$ and 61 configurations from Fig. 2 shown with all the B segments and the interfacial A segments stripped away. The ordered phase at $\chi N=61$ is cylindrical (C) as demonstrated by the two side views.

This is better demonstrated in Fig. 3, where all the B segments are deleted along with the interfacial A segments (defined as those with six or less A-type neighbors). This reveals a defect-free cylindrical morphology with approximate hexagonal symmetry at $\chi N=61$, in contrast to the highly irregular domains observed at $\chi N=60$.

The order parameter ψ defined in Eq. (4) is, by far, the most sensitive of our quantities for detecting the ordering/disordering of the microdomains. The effectiveness of ψ is illustrated in Fig. 4, where it is plotted for temperature scans back and forth across the ODT at three different molecular weights. The transition in Figs. 2 and 3 shows up in the heating curve of Fig. 4(b) as a jump of $\Delta\psi=0.0056$. Although the jumps in ψ are significantly smaller than previously observed for lamellar-forming diblocks,[19] they still display a well-pronounced hysteresis loop, signifying a discontinuous transition; the true position of the ODT generally occurs somewhere within the loop. The width of the hysteresis loops are recorded in Table I for four different system sizes at each of the three molecular weights.

The round brackets in Table I for $N=40$ and $L=64$ denote that the simulation behaved differently than the others. Specifically, it never fully ordered during the cooling run, but instead ordered in the heating run at $\chi N=62$. Nevertheless, we still regard this value as an upper bound for the ODT, because the system presumably would not have ordered unless that was the more stable state. In the following section, we encounter further examples of this delayed ordering, where we demonstrate that it results from the chance formation of a highly metastable defect or grain boundary.

The positions of the hysteresis loops are reasonably consistent among the different system sizes L, apart from the smallest ones. We attribute this to significant finite-size effects and therefore disregard those simulations. We also find no discernible variation in the positions of the loops as the molecular weight is changed; they all suggest an ODT of $(\chi N)_{\mathrm{ODT}}=60\pm2$. This lack of any significant molecular-weight dependence is reminiscent of the previous study at $f=0.5$,[19] where the same range of N displayed a relatively fixed ODT of $(\chi N)_{\mathrm{ODT}}=40\pm1$.

B. Internal energy

The $\chi N=36$ configuration in Fig. 2 illustrates a significant degree of microphase separation deep within the disor-

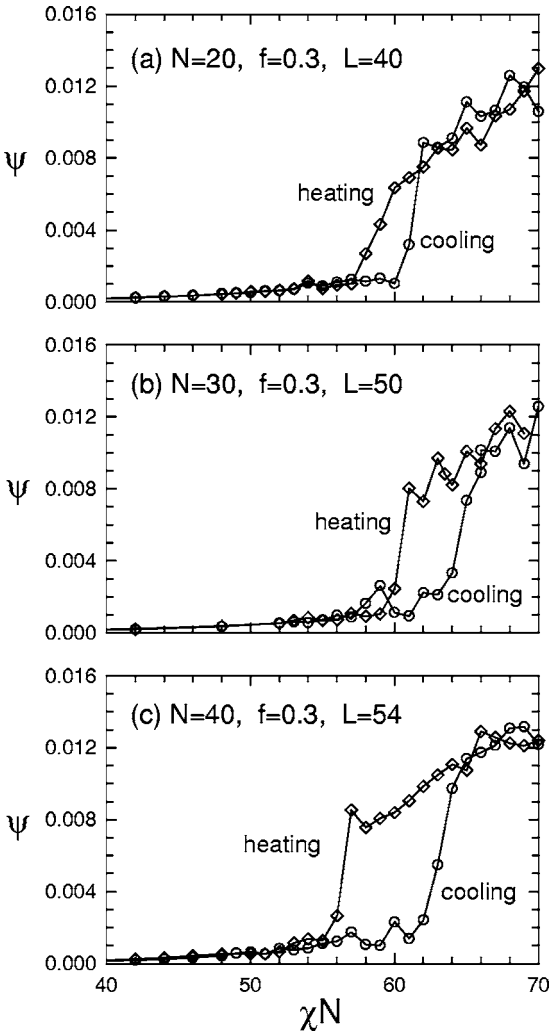

FIG. 4. Order parameter ψ from Monte Carlo runs where the system is cooled from $\chi N=0$ into the ordered cylindrical phase and then heated back into the disordered state. Results are presented for three degrees of polymerization: (a) $N=20$, (b) $N=30$, and (c) $N=40$.

dered phase, contrary to the uniform mixing predicted by mean-field theory. The degree of microdomain formation is most easily investigated by examining the reduction in the average number of A/B contacts $\langle n_{AB}\rangle$, which is directly proportional to the internal energy of the melt $U=\epsilon_{AB}\langle n_{AB}\rangle$. The actual reduction in $\langle n_{AB}\rangle$ is displayed in Fig. 5(a) for molecules of $N=20$, 30, and 40. Just as for symmetric diblocks,[19]

TABLE I. Monte Carlo ODT's for a diblock composition of $f=0.3$, and three different degrees of polymerization, $N=20$, 30, and 40. Each molecular weight is examined with four different system sizes L. Round brackets denote that the system did not fully order until the heating cycle.

N	$(\chi N)_{\mathrm{ODT}}$			
	$L=24$	$L=32$	$L=40$	$L=48$
20	50–54	58–61	58–61	61–63
	$L=30$	$L=40$	$L=50$	$L=60$
30	52–56	58–61	60–65	56–58
	$L=34$	$L=44$	$L=54$	$L=64$
40	52–56	58–62	56–63	56–(62)

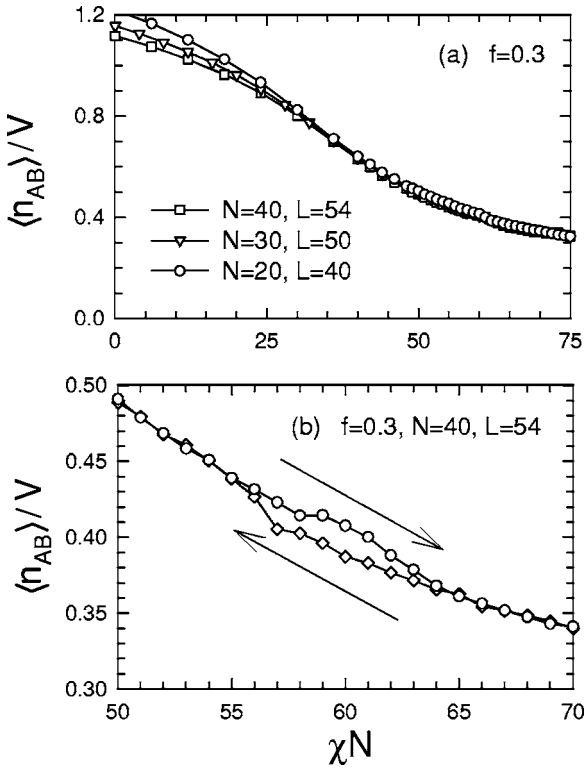

FIG. 5. (a) Average number of A/B monomer contacts $\langle n_{AB}\rangle$ vs segregation χN obtained from Monte Carlo cooling runs for three different molecular weights. (b) Hysteresis loop produced by cooling ($\bigcirc$) and subsequent heating ($\diamond$) runs.

the results for the different molecular weights nearly collapse onto a single curve when plotted as a function of χN. In each case, there is a $\sim 60\%$ reduction in AB contacts as the system evolves from infinite temperature ($\chi N=0$) to the ODT ($\chi N\approx 60$), which is in stark contrast to the constant level of $\langle n_{AB}\rangle/V=1.61$ assumed by uniform mixing.

At the resolution of Fig. 5(a), the cooling and heating curves appear virtually indistinguishable, but a closer examination shows a small hysteresis loop, as demonstrated by Fig. 5(b) for the case of $N=40$. Notice that the position of the loop perfectly matches that of the order parameter in Fig. 4(c). This loop in $\langle n_{AB}\rangle$ is similar to the previous ones observed at $f=0.5$,[19] but the separation between the cooling and heating curves is now considerably smaller.

In the previous study for $f=0.5$,[19] the small, but sudden, jumps in internal energy resulting from phase transitions created spikes in the heat capacity C_V. Notably, there was a significant variation in the strength of the peak, presumably depending on whether the transition occurred more within the equilibrating MCS or the statistics-collecting MCS. Apart from the occasional instances, where the transition was essentially complete by the end of the equilibration period, the spike was sufficiently strong so as to provide an unequivocal signature of the ODT. However, this is no longer true for $f=0.3$. At this composition, the change in internal energy seems to be either too small or too gradual to produce a definitive indicator of the ODT. Although there are often small peaks that accompany the phase transitions, they no longer dwarf those produced by the random thermal fluctuations.

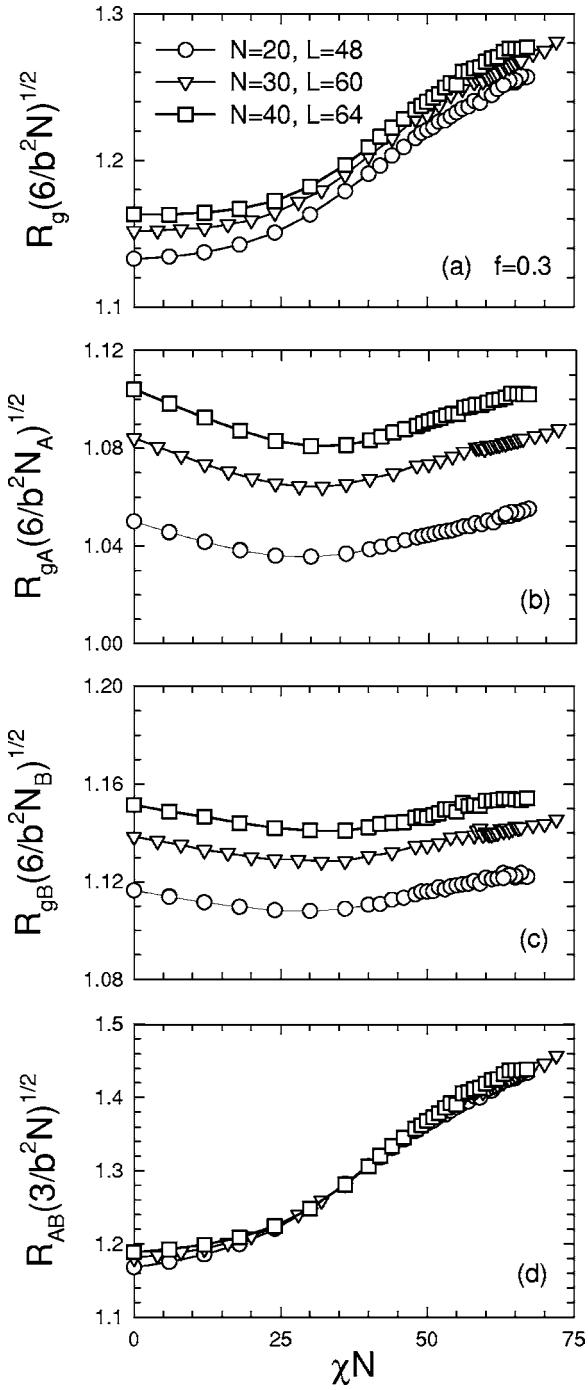

FIG. 6. Radii of gyration evaluated for (a) an entire molecule R_g, (b) an A block R_{gA}, and (c) a B block R_{gB}. (d) Separation between the A and B block centers of mass R_{AB}. Each quantity is plotted relative to its mean-field value corresponding to random-walk statistics (Ref. 19).

C. Dimensions of an individual molecule

The formation of A- and B-rich microdomains within the disordered state will naturally be accompanied by a distortion in the average polymer configuration. The actual degree of chain stretching is examined in Fig. 6 by displaying the radii of gyration of the entire molecule R_g and those of the two individual blocks $R_{g,A}$ and $R_{g,B}$, as well as the separation between the centers of the two blocks R_{AB}. Each of the quantities is plotted relative to the value predicted by random-walk statistics.[19] Because this ignores the self-avoidance, the curves start from values greater than 1 even in the athermal limit of $\chi N=0$. The issue, however, is the extra degree of stretching that occurs as χN increases from zero to the ODT at $\chi N \approx 60$. All three molecular weights show a similar increase of $\sim 10\%$ in the overall radius of gyration. As demonstrated by the remaining three plots, this is not a uniform stretching, but rather a displacement between the centers of mass of the A and B blocks by $\sim 20\%$ that occurs without a significant change in the size of each individual block. Again, the behavior is remarkably similar to that exhibited by symmetric molecules.[11,19]

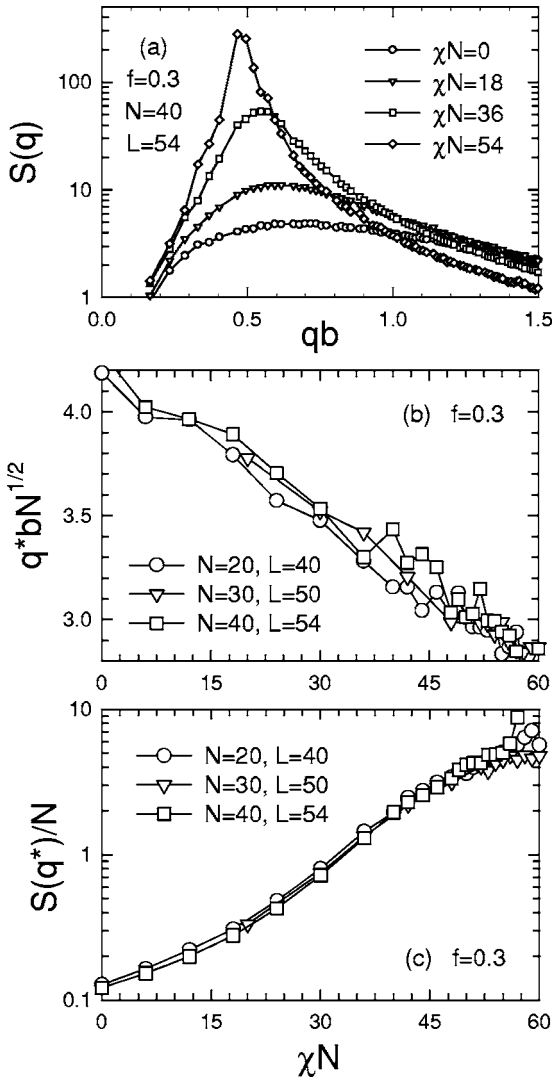

FIG. 7. (a) Structure function $S(q)$ plotted against wave number q at a series of segregations from disordered melts containing diblocks of $N_A=12$ and $N_B=28$. (b) Peak position q^* and (c) height $S(q^*)$ plotted as a function of segregation χN for three different molecular weights, $N=20$, 30, and 40.

D. Structure function

Experiments[10] are unable to explicitly observe chain stretching within the disordered state and instead access it by the less direct means of measuring the structure (or scattering) function $S(q)$. Figure 7(a) shows typical structure functions at several values of χN within the disordered phase, taken during one of our cooling runs involving diblocks of $N=40$ and $f=0.3$ on a lattice of size $L=54$. It displays the

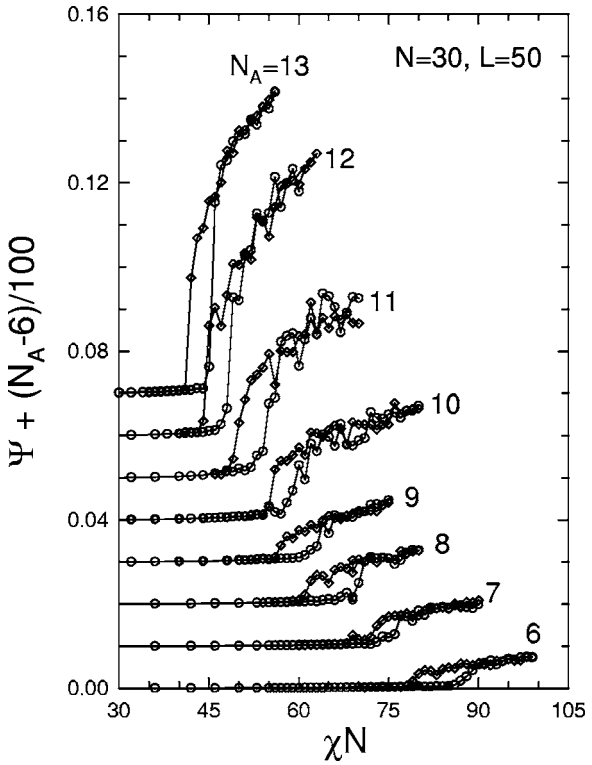

FIG. 8. Order parameter for cooling (◯) and heating (◇) runs for a series of compositions, N_A, obtained from diblock copolymer of size $N=30$ in a simulation box of size $L=50$.

usual peak, $S(q^*)$, at a wave number q^*, corresponding to an average separation between A and B segments of $2\pi/q^*$. Figure 7(b) plots the peak position q^* as a function of χN for three different molecular weights. As with the radius of gyration R_g, the results approximately collapse onto a single curve when scaled with respect to $bN^{1/2}$ and χN. In this case, q^* decreases by ~33% from $\chi N=0$ to 60 (the approximate ODT), which is significantly more than the corresponding increase in R_{AB}. As Fried and Binder[11] have pointed out, this implies that the shift in the peak position of $S(q)$ is due to more than just simple chain stretching; there must also be a cooperative (or collective) organization of the molecules for q^* to change faster than R_{AB}. For completeness, Fig. 7(c) also plots the peak amplitude, $S(q^*)$, as a function of χN for $N=20$, 30, and 40. As shown before,[19] the curves approximately collapse onto each other when $S(q^*)$ is divided by the molecular weight N. It is also interesting that the semilogarithmic plots are nearly linear, which corresponds to an exponential-like growth in the peak height with respect to χN.

IV. RESULTS FOR *N*=30 DIBLOCK COPOLYMERS

Here we construct a partial phase diagram for $N=30$ diblock copolymers over the composition range $0.2 \leqslant f \leqslant 0.8$. Highly asymmetric compositions are excluded because we take the position of Binder and Fried[14] that blocks with fewer than six segments lose their polymeric behavior. Figure 8 shows the order parameter for a series of simulations from $N_A=6$ to 13, using a lattice of size $L=50$. Runs were also performed at $N_A=14$ and 15 but have been omitted from Fig. 8 for reasons of clarity. Of course, it is redundant to perform runs for $N_A>15$ because of the symmetry with respect to the interchange of the A and B labels. At each composition, the heating/cooling temperature sweeps produced a well-defined hysteresis loop, locating the ODT in the reasonably narrow χN intervals listed in Table II. For the relatively symmetric compositions indicated by asterisks in Table II, we observed large peaks in the heat capacity C_V accompanying the sudden changes in the order parameter, similar to those reported previously for $f=0.5$.[19] As in the previous section for $f=0.3$, the more asymmetric molecules often produced small peaks, but not sufficiently strong so as to provide an unequivocal indicator of the transition.

TABLE II. Monte Carlo ODT's for diblock copolymer molecules of $N=30$ at various compositions, $N_A=6$ to 15, each examined with two different system sizes, $L=50$ and 60. Asterisks indicate transitions that were accompanied by a pronounced spike in the heat capacity, and round brackets denote those simulations where the system did not fully order until the heating cycle.

	$(\chi N)_{\mathrm{ODT}}$	
N_A	$L=50$	$L=60$
15	39*–41*	39*–43*
14	40*–44*	40*–44*
13	42–45*	41*–45*
12	44*–47	46*–(58)
11	49–54	50–(68)
10	56–59	···
9	57–62	56–(62)
8	61–68	59–65
7	68–74	66–74
6	79–87	80–(96)

Based on the comprehensive investigation at $f=0.3$ in Sec. III and $f=0.5$ in Ref. 19, $L=50$ should be sufficient to avoid any significant finite-size effects. Nevertheless, we have repeated the simulations in Fig. 8 using a larger lattice of $L=60$. As expected, the locations of the ODT, tabulated in Table II, are consistent with those of the smaller system size. However, runs on the larger lattice resulted in four more instances ($N_A=6$, 9, 11, and 12) where the system did not fully order until the heating cycle and in one instance ($N_A=10$) where it never completely ordered at all.

Figure 9 shows the behavior of the order parameter ψ at $N_A=12$. In this run, a metastable grain boundary occurred as the system tried to form a lamellar phase, and it did not anneal out until the heating cycle as indicated by the sudden rise in the order parameter at $\chi N=58$. This is confirmed by the side view in Fig. 10 of the minority A-type lamellae immediately before ($\chi N=60$) and after ($\chi N=58$) the disappearance of the grain boundary. The increased occurrence of highly metastable defects is attributed to the larger system size coupled with a larger step size in χN. [In order to save time, the step size for these runs was increased to $\Delta(\chi N)=2$.] Naturally, the larger lattice increases the chance of forming a defect, while the faster temperature sweep provides less time for it to anneal out. The chance occurrence of these defects is illustrated by the inset of Fig. 9, where the order parameter is plotted for four equivalent cooling runs all

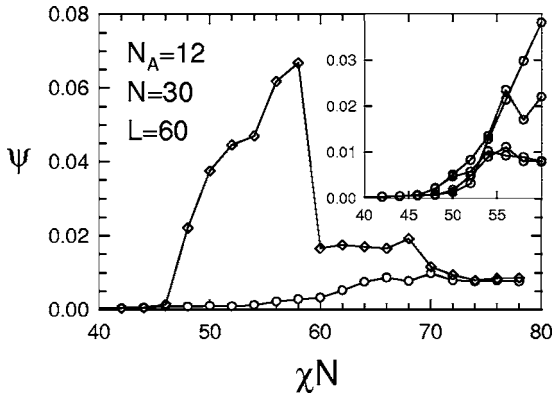

FIG. 9. Order parameter for cooling (◯) and heating (◇) runs for diblocks of $N_A=12$ and $N_B=18$ contained in a simulation box of size $L=60$. The inset shows the order parameter of four additional cooling runs all starting from the same initial configuration at $\chi N=40$, but with different random seeds.

starting from the exact same $\chi N=40$ configuration, but using different random seeds. Two runs show a sizable rise in the order parameter near $\chi N=54$ and go on to form well-ordered lamellar structures, while the other two develop significant defects capable of surviving high degrees of supercooling. Although not nearly to the same extent, some variation also occurs in the order-to-disorder transition between equivalent runs, as evident when comparing the $N=30$ and $N_A=9$ results from Tables I and II, respectively.

The ordered morphology above the ODT was visually identified at each composition. From $N_A=6$ to 9, the system formed the cylindrical (C) structure, and from $N_A=11$ to 15, it exhibited a simple lamellar (L) structure. In between, at $N_A=10$, we observe the formation of a complex morphology, specifically the perforated-lamellar (PL) phase. Figure 11 shows a configuration of the $L=50$ simulation box displaying a lamellarlike morphology at $\chi N=70$, but with breaks in the (dark) minority-component layers. To the right is a second image with the front segments removed so as to show a cut through the center of a minority layer. This reveals a close-packed array of perforations through which the (light) majority-component domain passes. Our $N_A=10$ simulation on the larger $L=60$ lattice also displayed a clear PL structure, but one with a grain boundary similar to that in Fig. 10.

The position of the hysteresis loop and the identification of the ordered phases is summarized in the phase diagram presented in Fig. 12. Following the standard dilution approximation,[24] an effective interaction parameter $\chi_{\text{eff}} \equiv \chi\phi_c$ has been introduced to account for our use of vacancies. Nevertheless, one still needs to be aware of the difference between the lattice and continuum definitions of χ, when comparing to Fig. 1. The mean-field critical point for the present lattice model occurs at $\chi_{\text{eff}}N=11.734$,[19] whereas $\chi N=10.495$ for the continuum model.[9] In any case, fluctuations have produced a sizable shift in the ODT towards higher χN and have also created direct transitions between the disordered state and the various ordered phases consistent with the experimental diagram of Fig. 1(a). As in experiments,[4] the PL phase is not necessarily the true equilibrium morphology; we will discuss this issue in the next section.

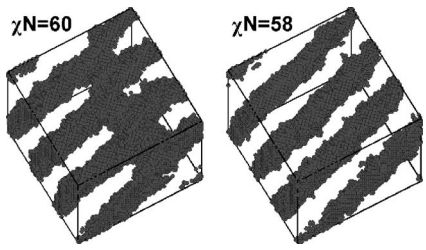

FIG. 10. Configurations from the heating run in Fig. 9 showing the minority-component A segments (for added clarity, the interfacial A segments have again been removed). The lamellar structure at $\chi N=60$ exhibits a grain boundary that anneals out by $\chi N=58$.

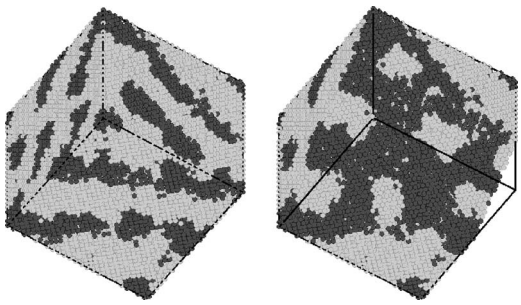

FIG. 11. Configuration of a perforated-lamellar (PL) phase obtained from a diblock copolymer melt with a composition of $N_A=10$ and $N_B=20$ and a segregation of $\chi N=70$ in a simulation box of size $L=50$. The configuration is repeated to the right, but with the front segments removed to reveal perforations through minority-component lamellae.

V. DISCUSSION

Our thorough study on disordered asymmetric diblocks of $f=0.3$ showed a remarkably similar behavior to that observed in previous studies[11,19] on symmetric diblocks of $f=0.5$. Again, the segregation of A and B segments began deep in the disordered region, as evident from the configurations shown in Fig. 2 as well as from the substantial reduction in A/B segment contacts plotted in Fig. 5. This segregation also polarized the diblock copolymers in the same manner, where the centers of mass of the two blocks sepa-

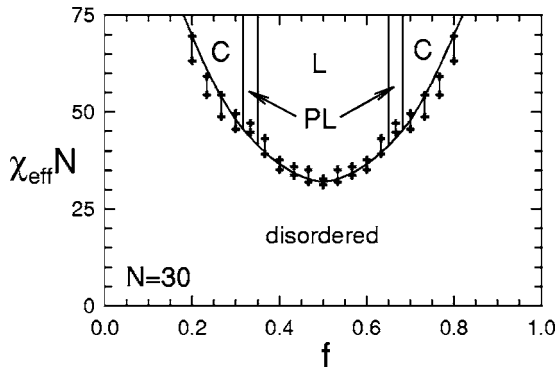

FIG. 12. Monte Carlo phase diagram showing the location of the ODT and identifying the ordered phases: lamellar (L), perforated-lamellar (PL), and cylindrical (C). The error bars at each composition represent the width of the hysteresis loop; the solid curves simply serve as convenient guides to the eye. An effective interaction parameter $\chi_{\text{eff}} \equiv \chi\phi_c$ is used to account for the presence of vacancies in the simulations, but no attempt is made to account for the slight difference between the lattice and continuum definitions of χ necessary for a quantitative comparison with Fig. 1.

rated without any significant increase in their individual radii of gyration. The *A*- and *B*-rich domains also displayed the same steady growth over the full range of χN, as indicated by the structure-function peak plotted in Fig. 7(b). Furthermore, our new $f=0.3$ results exhibited the same molecular-weight dependencies observed for the $f=0.5$ study in Ref. 19. With such consistency between the $f=0.3$ and 0.5 results, we can reasonably assume that this behavior of the disordered phase is general to all compositions, except perhaps at the extremes, $f\to 0$ or 1.

As expected, the treatment of fluctuation effects results in direct first-order transitions from the disordered state to the ordered nonspherical morphologies (i.e., L, PL, and C), contrary to the mean-field prediction in Fig. 1(b) and consistent with the experimental diagram in Fig. 1(a). The only qualitative difference with experiment is our lack of a gyroid (G) phase. Experiments[4] have, in fact, demonstrated that a metastable PL can readily form in place of G, presumably, because they have such similar free energies as supported by mean-field calculations.[25] It is likely that G is also more stable than PL in the present lattice model, but does not appear due to the finite-size and/or nonequilibrium effects in our simulations. First of all, the cubic unit cell of G is expected to be approximately $\sqrt{6}=2.449$ times the size of the lamellar period,[25] and thus would experience much greater difficulty adjusting to the finite-sized simulation boxes. Second of all, the minority domain of PL involves a far less intricate network compared with that of G, and thus may be nucleated from the disordered phase more frequently despite a slightly higher free energy. Once PL forms, the time scale required for it to convert to a more stable G phase would certainly exceed that of our simulations, much like the situation that occurs in experiments.[4]

Fluctuations are also expected to push $(\chi N)_{\mathrm{ODT}}$ to higher values as N decreases, but this effect is difficult to demonstrate, particularly in a quantitative manner. Even though the effect appears evident from the available experimental phase diagrams,[2] this is not the case. Experiments generally determine the temperature dependence of χ by fitting to the Fredrickson-Helfand (F-H) theory,[8] which predisposes a shift in the ODT. Simulations suffer the problem that the effect is too gradual to be detected directly from the assessable range of N. As with other Monte Carlo studies for $f=0.5$, our $(\chi N)_{\mathrm{ODT}}$ values for $f=0.3$ show no discernible variation over the range $N=20-40$. It is also difficult to infer a shift based on comparisons to the mean-field diagram in Fig. 1(b), which is understood to represent the $N\to\infty$ limit, because of the differences in the definition of χ. Many simulation studies[15,20,21] define an effective χ in an attempt to make quantitative comparisons with the F-H theory, but the results are highly sensitive to the chosen definition,[26] and so such comparisons are contentious. Therefore, we make no such attempt. In any case, the F-H theory is only intended to apply for $\bar{N}\gtrsim 10^6$,[8] while simulations are generally restricted to $\bar{N}\lesssim 10^2$,[19,27] where $\bar{N}$ is the invariant polymerization index. Furthermore, the quantitative predictions of the F-H theory are highly questionable in light of Ref. 12. In our opinion, the best evidence for a fluctuation-induced shift in the ODT is the direct comparison with mean-field calculations performed on the equivalent fcc lattice model, which predicts the mean-field critical point for symmetric diblocks at $\chi N=14.667$ far below the actual ODT at $\chi N=40\pm 1$.[19]

Although simulations on asymmetric diblock copolymer melts are scarce, there are several relevant studies. The earliest, by Binder and Fried,[14] examined a similar model, but with a simple cubic lattice. Focusing on the single composition $f=0.25$, with three molecular weights, $N=24$, 32, and 40, they evaluated the structure function and single-chain dimensions throughout the disordered state and found results analogous to ours. Although they identified the ordered phase as cylindrical (C), they were unable to detect any signature of the ODT. Micka and Binder[16] revisited the problem, attempting to use finite-size-scaling techniques to locate the ODT, but with no success. They attributed the failure to the nontrivial scaling behavior associated with the general incommensurability of the natural periodicity of the C phase and the size of the simulation box. Another problem they may have not appreciated at that time is the strength of the first-order transition, as evident from the high degree of segregation in the $\chi N=61$ (ordered state) configuration of Fig. 2; finite-size-scaling techniques are designed for second-order or, at least, weakly first-order transitions.

A couple of years later, Pakula *et al.*[20] examined $N=40$, $f=0.25$ diblock copolymers with the exact same fcc lattice model as ours, but using a cooperative motion algorithm that allowed them to remove the vacancies (i.e., $\phi_c=1.0$). They only performed one cooling run, which exhibited a well-defined spike in the heat capacity C_V, at $\chi N=46$ [using the definition in Eq. (1)]. Their ordered cylindrical (C) morphology is consistent with our phase diagram in Fig. 12, but the position of the ODT is slightly less than our estimate of $\chi_{\mathrm{eff}}N=50$. This could be attributed to inaccuracies in the dilution approximation,[24] but it is more likely a consequence of their relatively small lattice, $30\times 30\times 40$, which was presumably a necessity of using their more complex Monte Carlo algorithm. Indeed, our simulations on the small system sizes in Table I experienced similar shifts in the ODT.

Also at about the same time, Hoffmann *et al.*[17] examined $N=24$ and $N=32$ diblocks, each at three different asymmetric compositions. They did not find any peaks in the heat capacity, but they did observe the apparent onset of higher-order Bragg reflections in the structure function $S(q)$. However, this did not provide a particularly clear indication of the ODT, nor was it particularly convincing. They struggled to index the Bragg reflections and did not provide identification of their ordered morphologies.

Perhaps the most extensive study of asymmetric diblocks, next to ours, is that by Schultz *et al.*[27] They performed off-lattice molecular-dynamics simulations, although on systems of fewer molecules and lower molecular weights ($N=10$ and 20). Furthermore, their simulations were conducted at relatively low packing fractions (i.e., $\phi_c<0.5$), which make their results more relevant to concentrated block copolymer solutions as opposed to melts. Nevertheless, their simulations produced the same morphologies, L, PL, and C, and a couple of their highly asymmetric compositions ($f=0.1$) also displayed spheres (S). Interestingly, their PL

morphology seems to occupy a much larger region of the phase diagram compared with the PL morphology in our study; nevertheless, it too could be a metastable phase that occurs in place of the G phase due to finite-size effects.

Our particular study has various strengths over the preceding ones. First of all, we only considered sufficiently large N such that neither block had fewer than six segments, whereas, for example, some of the simulations in Ref. 27 involved blocks containing only a single monomer. In such extremes, the block has absolutely no configurational entropy and is thus no longer polymeric. Second of all, we experimented with a range of system sizes to ensure that our results were not significantly influenced by finite-size effects, whereas, for example, the ODT in Ref. 20 likely experienced a significant shift due to their use of a small simulation box. Third of all, we had an effective order parameter that provided us with a definitive signature of the ordering and disordering transitions. Lastly and perhaps most importantly, we performed the heating and cooling runs necessary to produce the hysteresis loops characteristic of first-order transitions. The fact that the hysteresis loops are closed provides strong evidence that the system is in equilibrium outside the loops, while at the same time it provides upper and lower bounds for the ODT.

VI. SUMMARY

A Monte Carlo study of diblock copolymer melts has been performed using a three-dimensional fcc lattice model. The first part of the study involved extensive simulations on cylinder-forming molecules with composition $f=0.3$, analogous to the previous work on lamellar-forming molecules with $f=0.5$. Three separate molecular weights, $N=20$, 30, and 40, were examined, each over a series of different-sized simulation boxes so as to assess finite-size effects. The product χN was found to be a good scaling variable for the molecular-weight dependence of our results. Large fluctuation effects extending throughout the entire disordered phase from $\chi N=0$ to the ODT at $(\chi N)_{\mathrm{ODT}}=60\pm2$ were observed. The significant departure from mean-field theory was manifest in a $\sim$60% reduction in internal energy, a $\sim$20% stretching in the intramolecular center-of-mass separation of the A and B blocks, and a $\sim$33% increase in the domain size associated with the peak q^* of the scattering function $S(q)$. All these results were quantitatively similar to those of the previous studies at $f=0.5$ in Refs. 11 and 19, suggesting that the behavior extends over the entire composition range with perhaps the exception of highly asymmetric copolymers.

The second part of our study focused on $N=30$ diblock copolymers and located the ODT over a wide range of compositions, $0.2\leqslant f\leqslant 0.8$, allowing us to construct the Monte Carlo phase diagram in Fig. 12. This mapping of the ODT was facilitated by a recently discovered order parameter that produces a clear hysteresis loop. In contrast to the mean-field prediction in Fig. 1(b), direct first-order transitions from disordered melts to lamellar (L), cylindrical (C), and perforated-lamellar (PL) morphologies were clearly identified, analogous to those observed in the experimental diagram of Fig. 1(a). However, we suspect that, much like in experiments, the PL morphology occurs in place of a more stable gyroid (G) morphology due to nonequilibrium effects that are also exacerbated by the finite size of our simulation boxes.

ACKNOWLEDGMENTS

One of the authors (M.W.M.) received funding for this project from EPSRC (GR/N36721), while another author (R.W.) was supported by NSERC, CFI, and AIF. The latter also thanks Stephen Condran and Doug Hunter for their useful help and acknowledges Greg Lukeman and the StFX hpcLAB for computing resources.

[1] F. S. Bates and G. H. Fredrickson, Phys. Today **52**, 32 (1999).
[2] F. S. Bates, M. F. Schulz, A. K. Khandpur, S. Förster, J. H. Rosedale, K. Almdal, and K. Mortensen, Faraday Discuss. **98**, 7 (1994).
[3] M. W. Matsen and F. S. Bates, Macromolecules **29**, 1091 (1996).
[4] D. A. Hajduk, H. Takenouchi, M. A. Hillmyer, F. S. Bates, M. E. Vigild, and K. Almdal, Macromolecules **30**, 3788 (1997).
[5] M. W. Matsen and F. S. Bates, J. Polym. Sci., Part B **35**, 945 (1997).
[6] S. A. Brazovskii, Sov. Phys. JETP **41**, 85 (1975).
[7] N. Sakamoto, T. Hashimoto, C. D. Han, D. Kim, and N. Y. Vaidya, Macromolecules **30**, 1621 (1997); J. F. Wang, Z.-G. Wang, and Y. L. Yang, *ibid.* **38**, 1979 (2005).
[8] G. H. Fredrickson and E. Helfand, J. Chem. Phys. **87**, 697 (1987).
[9] L. Leibler, Macromolecules **13**, 1602 (1980).
[10] K. Almdal, J. H. Rosedale, F. S. Bates, G. D. Wignall, and G. H. Fredrickson, Phys. Rev. Lett. **65**, 1112 (1990).
[11] H. Fried and K. Binder, J. Chem. Phys. **94**, 8349 (1991); Europhys. Lett. **16**, 237 (1991).
[12] A. Kudlay and S. Stepanow, J. Chem. Phys. **118**, 4272 (2003).
[13] G. H. Fredrickson, V. Ganesan, and F. Drolet, Macromolecules **35**, 16 (2002); M. Müller and F. Schmid, Adv. Polym. Sci. **185**, 1 (2005).
[14] K. Binder and H. Fried, Macromolecules **26**, 6878 (1993).
[15] R. G. Larson, Macromolecules **27**, 4198 (1994).
[16] U. Micka and K. Binder, Macromol. Theory Simul. **4**, 419 (1995).
[17] A. Hoffmann, J.-U. Sommer, and A. Blumen, J. Chem. Phys. **107**, 7559 (1997).
[18] A. Weyersberg and T. A. Vilgis, Phys. Rev. E **48**, 377 (1993); A. Hoffmann, J.-U. Sommer, and A. Blumen, J. Chem. Phys. **106**, 6709 (1997).
[19] O. N. Vassiliev and M. W. Matsen, J. Chem. Phys. **118**, 7700 (2003).
[20] T. Pakula, K. Karatasos, S. H. Anastasiadis, and G. Fytas, Macromolecules **30**, 8463 (1997).
[21] W. H. Jo and S. S. Jang, J. Chem. Phys. **111**, 1712 (1999).
[22] M. W. Matsen, J. Phys.: Condens. Matter **14**, R21 (2002).
[23] D. P. Landau and K. Binder, *A Guide to Monte Carlo Simulations in Statistical Physics* (Cambridge University Press, Cambridge, 2000).
[24] J. R. Naughton and M. W. Matsen, Macromolecules **35**, 5688 (2002).
[25] M. W. Matsen and F. S. Bates, J. Chem. Phys. **106**, 2436 (1997).
[26] Q. Wang, P. F. Nealey, and J. J de Pablo, Macromolecules **35**, 9563 (2002).
[27] A. J. Schultz, C. K. Hall, and J. Genzer, J. Chem. Phys. **117**, 10329 (2002).